

Combinatorial Multiplex Assay Format Using Electronic Microchip Arrays and Its Potential Application in Complex Cancer Diagnostics, Phillip S. Kim,^{*} Denice K. Tai, and Kan V. Lu (KnowledGENE, Inc., Department of Research and Development, 13206 Estrella Ave., Suite C, Gardena, CA 90248; ^{*} author for correspondence: fax 310-533-0506, e-mail pkim@knowledgene.com)

A key challenge in cancer treatment and prevention is early disease detection, thus facilitating effective therapeutic intervention to improve quality of life and survival. With molecular genetics playing an increasingly important role in solid tumor diagnostics, the identification of biomarkers that act as signatures of specific cancers at various developmental stages is critical to enable early definitive detection and diagnosis (1). Established cancer biomarkers can be quickly screened and detected by sensitive molecular genotyping to assess cancer risk and afford the earliest therapeutic intervention possible. Such biomarkers may also render meaningful prognostic information as well as assist in the selection of individual treatment regimens. As cancer biomarkers are discovered and characterized, the ability to quickly and economically screen large numbers of patients for a wide variety of markers is essential. This capability is further underscored by the complex and varied mutation profiles associated with cancer markers.

In the present study, a combination of well-characterized gene mutations encompassing single-nucleotide polymorphisms, microdeletions, and insertions commonly found in the gene encoding the cystic fibrosis transmembrane conductance regulator (*CFTR*) was used to provide proof of principle for a method capable of simultaneously identifying multiple specific alleles by use of electronically controlled microchips. Mutation regions are amplified and applied to a single microchip test site addressed with multiple biotinylated oligonucleotide cap-

ture probes. Fluorescently labeled reporter probes specific to wild-type or mutant alleles are then hybridized to the complex to provide precise genotyping. This method does not identify, but only detects the presence of any mutant alleles in a specimen; however, it permits the simultaneous screening of a large cohort of patients for a large number of different mutations. This rapid high-throughput screening platform, designated combinatorial multiplexing, can be applied to any disease-associated genes or biomarkers, especially those with complex genotype profiles, to aid in clinical diagnosis.

We selected 11 well-characterized mutations encompassing seven regions in *CFTR* and designed primers for PCR amplification based on sequences obtained from GenBank (accession nos. M55106–M55131). The primer sequences are listed in Table 1. Mutations examined were G085E, 405+3A→C, 711+1G→T, R334W, R347H, R347P, A455E, ΔF508, 2184delA, 2307insA, and 3659delC (2). Each amplicon was amplified from 15 ng of genomic DNA in a 50-μL reaction consisting of 1× PCR buffer (Invitrogen), 1.8 mM MgCl₂, 400 μM deoxynucleotide triphosphates, 400 nM each primer, and 5 U of Platinum *Pfx* DNA polymerase (Invitrogen). Thermal cycling conditions were as follows: 95 °C for 3 min; 35 cycles of 95 °C for 30 s, 55 °C for 30 s, and 72 °C for 45 s; and final extension at 72 °C for 2 min. PCR products were desalted through Multiscreen-PCR filter plates (Millipore) and analyzed on 1.5% agarose gels.

Capture oligonucleotides specific for each selected mutation were synthesized with 3' biotinylated ends to permit permanent addressing onto Nanochip™ (Nanogen) arrays, which feature a protective agarose permeation layer containing streptavidin (3). Capture and reporter oligonucleotides were designed to permit amplicon-directed juxtaposition of the 3'-terminal base of the reporter to the 5'-terminal base of the capture when a positive hybridization match occurs. This method takes advantage of the premise that base stacking stabilizes

Table 1. PCR amplicons and primer sequences.

PCR amplicon position	CF mutations covered	Primer sequences ^a	Amplicon size, bp
Exon 3–Intron 3	G085E, 405+3A→C	F: 5'-CGATGTTTTTCTGGAGATTTATGT-3' R: 5'-ATCCTTACTAGAGTTTTAGGTGGTT-3'	205
Exon 5–Intron 5	711+1G→T	F: 5'-GACAACCTGTTAGTCTCCTTTCC-3' R: 5'-ACATGTACGATACAGAATATATGT-3'	254
Exon 7	R334W, R347H, R347P	F: 5'-TGCACTAATCAAAGGAATCA-3' R: 5'-TCCTAGTATTAGCTGGCAA-3'	286
Exon 9	A455E	F: 5'-TACTCCTGTCCTGAAAGATA-3' R: 5'-TACACCCATACATTCTCCTA-3'	206
Exon 10	ΔF508	F: 5'-ATGATTATGGGAGAAGTGA-3' R: 5'-TATAATTTGGGTAGTGTGAAGGGT-3'	238
Exon 13	2184delA, 2307insA	F: 5'-AAAGAAGAAATTCATCCTAAC-3' R: 5'-AGTGTGTCATCAGGTTCCAGG-3'	365
Exon 19	3659delC	F: 5'-ATGCGATCTGTGAGCCGA-3' R: 5'-ATTTCCACCTCTGTGATTTTGTCT-3'	214

^a F, forward; R, reverse.

DNA hybridization such that matched reporter binding is preferentially more stable than mismatched reporter binding (4). Only in the presence of base stacking, when capture and reporter oligonucleotides are in direct apposition and paired to the patient amplicon, will the hybrid be stabilized. Capture/reporter allele sets were first individually assessed to confirm their ability to specifically detect and discriminate between mutant and wild-type specimens. Capture probes were diluted to a concentration of 0.5 $\mu\text{mol/L}$ in 50 mmol/L histidine and electronically addressed to selected sites on the microchip by use of mapping protocols created from instrument software (5). Sites were also biased with histidine alone to serve as background controls. Appropriate target amplicons were denatured at 95 °C for 5 min and quickly cooled on ice before hybridization. A 5- μL sample of each denatured amplicon in 50 mmol/L histidine was then electronically hybridized to the relevant capture-containing sites on the chip.

After amplicon hybridization, chips were manually washed three times with high-salt buffer [50 mmol/L sodium phosphate (pH 7.4), 500 mmol/L NaCl]. Pairs of allele-specific reporters labeled with either Cy3 (wild type) or Cy5 (mutant) fluorophore were mixed equally at 0.5 $\mu\text{mol/L}$ to yield a combined 1 $\mu\text{mol/L}$ in high-salt buffer. Reporter solutions were applied to the chip and hybridized passively for 3 min at room temperature, followed immediately by three more washes in high-salt buffer. Thermal discrimination and fluorescence detection were then performed in the fluorescent reader instrument. Chips were loaded into the reader and washed with low-salt buffer (50 mmol/L sodium phosphate, pH 7.4); an initial fluorescent image was then taken by use of separate lasers for each fluorophore. The capture/target/reporter complex was then thermally denatured to achieve precise discrimination between matched and mismatched alleles, followed by washes in low-salt buffer at the increased temperature. A final fluorescent scan of the array was taken, and background controls were subtracted from each pad's signal for final quantification. Optimal discrimination was achieved in all of the alleles at a temperature range of 27–28 °C.

When analyzing individual alleles, we scored fluorescence hybridization patterns by the criteria that wild-type samples meet or exceed a 5:1 threshold ratio of Cy3 to Cy5 signal, that heterozygous samples exhibit a 3:1 ratio in either direction, that homozygous mutant samples have a 5:1 ratio of Cy5 to Cy3 signal, and that the signal-to-noise ratios for any reporter be at least 5:1. These genotypes were assigned using the manufacturer's recommended biallelic fluorescence intensity ratios, and no genotype designations were made for fluorescence intensity ratios between 1:3 and 1:5. Homozygous wild-type alleles were all robustly bound by Cy3-labeled reporter, whereas homozygous mutant alleles were bound only by Cy5-labeled reporter. Heterozygous amplicons exhibited both Cy3 and Cy5 signals at equivalent intensities, identifying the presence of both wild-type and mutant alleles. Control captures hybridized to nonspecific amplicons or reporters

appropriately showed background fluorescence, demonstrating the high specificity of each individual capture/amplicon/reporter group. DNA samples with known cystic fibrosis mutations were previously genotyped and provided by ARUP Laboratories.

We next addressed arrays with diluted amounts of capture probes to simulate multiplexed assay conditions. Reduction of each capture's quantity volumetrically allows for more captures to be combined at once, while also lowering reagent cost. The increase in the number of different captures present is offset by the final molar quantity of each capture bound to the array surface. To assess assay sensitivity when captures are diluted out by competing captures, we addressed mixtures of two captures at molar ratios of 1:29 and 29:1 to simulate a potential 30-capture mixture. After hybridization of the captures' two corresponding wild-type amplicons, Cy3 fluorescence intensity for the more concentrated allele was robust, whereas signal intensity for the more dilute allele was slightly less but still unmistakably detectable. The same results were obtained when the molar ratios of the two captures were reversed and when different captures were used.

Multiplex assays were prepared by addressing nine different captures simultaneously onto single pads in which the concentration of each capture probe in the mixture was 83.3 nmol/L. A mixture of wild-type amplicons corresponding to all captures represented on the multiplexed sites was hybridized, and reporter sets were individually applied to assess each capture/amplicon/reporter hybrid independently. For each capture present in the multiplex, another multiplex pad in which that particular capture was absent from the mixture was prepared as a negative control for target specificity. For each multiplexed capture, the corresponding wild-type amplicon was detected and correctly genotyped, whereas the control multiplex pad (in which the capture in question was absent) exhibited fluorescence intensities near that of background. Systematic application of each reporter set in this manner confirmed the specificity of each capture/amplicon/reporter complex in a multiplex format. Use of heterozygous or mutant amplicons in the multiplex assay also led to their successful detection and accurate scoring as such, demonstrating that the multiplex format is capable of discriminating between genotypes. Fig. 1 shows the fluorescence patterns of various individual alleles in a heterozygous carrier for G085E in the multiplexed format.

Although this multiplex assay successfully combined 9 mutation alleles on a single test site, data from our experiments using diluted captures suggest that it is theoretically possible to screen for at least 30 mutations simultaneously without a considerable loss in assay sensitivity. Fluorescence intensity was reduced ~30% for a capture diluted 1:29 by a competing capture, but the signal-to-noise ratios remained >20:1 and fluorescence genotyping criteria were preserved. Because the objective of the multiplex screening assay is to simply detect the presence of any mutant alleles, the unambiguous strength

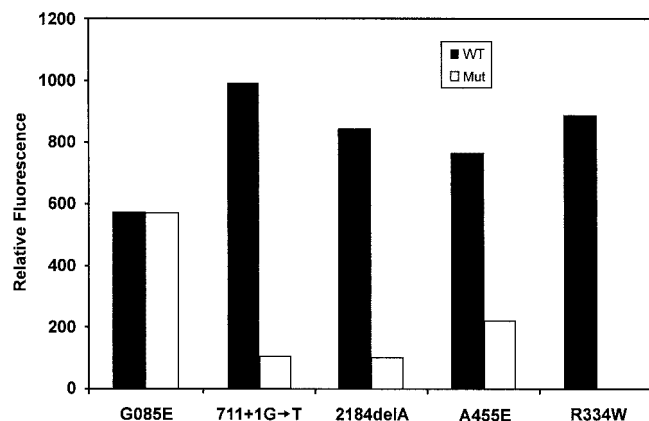


Fig. 1. Individual fluorescence patterns for alleles from an individual heterozygous for G085E by use of combinatorial multiplexing.

of a single positive mutant signal is sufficient to identify the presence of the mutation. To better circumvent potential problems associated with nonspecific oligonucleotide cross-hybridization in a highly complex mixture, however, it may be more practical to limit the number of mutations screened on a test site to 15, considering that each microchip array offers 100 sites.

Conventional methods of mutation detection are often time-consuming and laborious, making detection of diseases with complex mutation profiles a monumental task. Our results demonstrate that complex multiallelic mutation detection can be rapidly and accurately achieved on a prefabricated microchip array, making it highly amenable for routine detection of the diverse assortments of deleterious alterations found in many cancer markers and heritable diseases. Collectively, our methodology imparts several potential advantages over existing mutation detection systems, including high throughput and rapid turnaround, which may in turn lower genotyping costs.

In summary, combinatorial multiplexing is an efficient and, more importantly, accurate method for multiple mutation detection that allows for the potential to simultaneously and rapidly screen a large number of patients for the presence of many different mutations.

References

1. Srinivas PR, Kramer BS, Srivastava S. Trends in biomarker research for cancer detection. *Lancet Oncol* 2001;2:698-704.
2. Grody WW, Cutting GR, Klinger KW, Richards CS, Watson MS, Desnick RJ. Laboratory standards and guidelines for population-based cystic fibrosis carrier screening. *Genet Med* 2001;2:149-54.
3. Gilles PN, Wu DJ, Foster CB, Dillon PJ, Chanock SJ. Single nucleotide polymorphic discrimination by an electronic dot blot assay on semiconductor microchips. *Nat Biotechnol* 1999;17:365-70.
4. Radtkey R, Feng L, Muralidhar M, Duhon M, Canter D, DiPierro D, et al. Rapid, high fidelity analysis of simple sequence repeats on an electronically active DNA microchip. *Nucleic Acids Res* 2000;28:E17.
5. Edman CF, Raymond DE, Wu DJ, Tu E, Sosnowski RG, Butler WF, et al. Electric field directed nucleic acid hybridization on microchips. *Nucleic Acids Res* 1997;25:4907-14.

Rolling Circle Amplification Technology as a Potential Tool in Detection and Monitoring of Cancer by Flow Cytometry, Arumugham Raghunathan,* Martin P. Sorette, Harley R. Ferguson, Jr., and Steven P. Piccoli (Molecular Staging, Inc., Cellular Analysis Section, Flow Cytometry Group, 300 George St., Suite 701, New Haven, CT 06511; *author for correspondence: fax 203-776-5278, e-mail ragoor@molecularstaging.com)

Rolling circle amplification (RCA) generates a localized signal via isothermal amplification of an oligonucleotide circle reporter sequence. The application of this approach to flow cytometry could extend the utility of existing methods by enhancing the sensitivities and specificities for various applications, including early diagnosis of cancer and of hematologic and other abnormalities.

RCA technology is applicable to a variety of platforms for the simultaneous detection of molecules as a function of either antigenicity or nucleic acid sequence (1-4). In flow cytometry, cells of interest are characterized based on population gating. Efficient gating strategies are crucial for accurate immunophenotyping, more so in a heterogeneous cell suspension such as peripheral blood mononuclear cells (PBMCs). Usually a combination of light scatter (forward and side) and immunophenotypic markers is critical in identifying the specific cells of interest. A panel of antibodies is usually used to characterize a subset of cells based on their surface markers. However, cells can be best characterized only when the staining for each of these markers is bright enough to clearly differentiate them from unstained cells. This requires specific antibodies and intense detection signals. Abundantly expressed cell surface markers are not difficult to stain and identify compared with rare surface antigens, which are currently gaining importance in diagnostics and clinical studies. Therefore, the common challenge in clinical or diagnostic flow analysis is insufficient signal (low-intensity signals) leading to inefficient use of the existing antibody library.

RCA technology can help overcome these problems. The RCA technology (RCATTM) also allows for multiplexing or multiparametric analysis of various markers simultaneously, supporting the expanding use of complex marker panels for disease diagnosis and prognosis. RCA-mediated signal amplification has been successfully applied to the detection of cell surface antigens (e.g., CD4 and CD28) on PBMCs. This technical report describes the technology and protocol for flow cytometric analysis of lymphocyte surface markers. We have achieved a >10-fold increase in median fluorescent intensity (MFI) with RCA compared with conventional detection methods.

Human PBMCs were separated from whole blood by density gradient centrifugation using Vacutainer CPT tubes (Becton Dickinson). Two low-speed (300-400g) washes were performed in 1× phosphate-buffered saline (PBS; pH 7.4) to minimize platelet contamination. After centrifugation, cells were diluted to obtain ~5 × 10⁶ cells so that 100 μL would give 500 000 cells/sample.

Although this may be a limitation in studies requiring

recovery of viable cells, we found that cell fixation and permeabilization play an important role in cell staining and RCA. Although fixation was not absolutely necessary for amplification of signals, a light fixation substantially enhanced the efficiency of the subsequent RCA reaction. Therefore, for the studies described here, 500 000 cells were fixed with 5 g/L paraformaldehyde for 2 min at room temperature. The cells were then washed and blocked with 50 mL/L normal goat serum (NGS) in PBS, pH 7.4. An equal volume of 50 mL/L NGS, isotype controls (negative control samples), or 2 mg/L primary antibody (phycoerythrin-conjugated anti-CD4/CD28) diluted in 50 mL/L NGS was added to the cells and incubated in the dark for 30 min at room temperature. Alternatively, samples to be detected by second-step reagents were incubated with a biotinylated anti-CD4/CD28 antibody (30 min at room temperature), washed in PBS, and resuspended in a 1:1000 dilution of phycoerythrin-conjugated streptavidin (cat. no. S-866; Molecular Probes) for 15 min at room temperature (in the dark). After this incubation, cells were washed, centrifuged, and kept on ice until analysis by flow cytometry.

RCA. The blocked PBMCs were incubated with a preannealed complex of an anti-CD4–primer 4.2 conjugate [details of conjugates and circle are described in Gusev et al. (4)] and circle 4.2 in the conjugate-circle-complex diluent [C3-diluent; containing 150 mmol/L potassium glutamate, 10 mmol/L HEPES (pH 7.4), and 5 mL/L polyvinyl alcohol] for 30 min at room temperature. The negative controls were incubated with circle only (without conjugate) in the C3-diluent. Preannealing was done with 100 mg/L antibody conjugate and 2000 nmol/L DNA circle in the C3-diluent for 15 min at 37 °C, and the mixture was diluted 50-fold (in C3-diluent) before addition to cells. Alternatively, for indirect detection followed by RCAT analysis, the preannealed complex was prepared with an anti-biotin–primer 4.2 conjugate and circle 4.2, diluted 50-fold in C3-diluent, and added for 5 min at room temperature directly to PBS-washed cells that were incubated with a biotinylated primary antibody.

After the preannealed conjugate/circle incubations, the cells were washed and subjected to RCAT in the presence of 30 U of ϕ 29 polymerase per 25- μ L reaction volume. The reaction mixture contained 150 mmol/L potassium glutamate, 35 mmol/L HEPES (pH 7.4), 10 mmol/L magnesium acetate, 7 mmol/L dithiothreitol, 70 mg/L bovine serum albumin, and 400 μ mol/L each deoxynucleotide triphosphate. The reaction was incubated at 31 °C for 15 min. The cells were then centrifuged with an addition of 100 μ L of 50 mL/L NGS in PBS, pH 7.4, and decorated in 50 μ L of an 8 mg/L phycoerythrin–decorator complex in 50 mL/L NGS.

The decorator used was an oligonucleotide complementary to the DNA circle 4.2 and had a biotinylated thymidine at the 3' end with an eight-nucleotide spacer of deoxyinosine and deoxyuridine. This decorator was incubated with phycoerythrin-conjugated streptavidin overnight at 4 °C in PBS, pH 7.4, and purified on a size-exclusion column to remove the free constituents,

essentially as done by Davis et al. (5) with minor modifications.

Flow cytometry. Cells were analyzed by use of a Becton Dickinson FACSCalibur equipped with a 15 mW, 488 nm, air-cooled argon ion laser; a four-color analytical module; and a 635 nm red diode laser for Cy5 studies. Ten thousand events were acquired in list mode while gating lymphocytes and excluding debris. A histogram overlay of antibody fluorescence was constructed on the gated regions, and values for median channel fluorescence of CD4 expression were derived from the linear scale (1–10 000). The increase in amplification was calculated by the fold difference in the signal-to-noise ratios of conventional and RCAT detection. Data were analyzed using CELLQuest 3.3 (Becton Dickinson), WinMDI (freeware), and MS Excel.

During the development of the described protocol, a series of experiments were performed. Conditions for fixation of cells, application of RCA without destroying the antigenicity of cells, and the amplification step as such were adjusted to optimize the performance of the technology. We compared the proposed method with existing conventional detection methods to demonstrate the performance of the technology; experiments were repeated multiple times ($n = 54$ for CD4 and $n = 12$ for CD28 experiments) to determine reproducibility. Reproducibility was determined by the calculating the fold amplification (signal-to-noise ratio). The CV was <0.02%.

With conventional detection methods, the lymphocyte profile for CD4 is seen as a tight peak at the third log of signal intensity. When comparing MFIs with RCA, however, we saw a >10-fold increase in signal with minimal increase in the background peak in both the direct and indirect detection systems (Table 1 and Fig. 1).

CD4 is highly expressed (~98 000 molecules/cell), but only ~12 000 molecules of CD28 antigen are expressed in lymphocytes (6). Therefore, we chose CD28 as a second marker with moderate expression on a T-cell subset. Results showed a >10-fold increase in fluorescence intensity by signal amplification using RCA compared with conventional indirect detection using streptavidin-phycoerythrin (Table 1). Signal amplification was also effective with CD4 detection on monocytes (moderate expression, usually approximately one log lower than on lymphocytes), going beyond a 10-fold increase over direct labeling (data not shown).

Our results demonstrate the potential of RCAT in enabling the development of a next-generation tool for better detection and monitoring of cell surface markers in pathologic conditions by flow cytometry. This can be achieved because of the increased sensitivity that the technology offers to the process of signal amplification. Unlike PCR or tyramide signal amplification, RCA requires only a single round of amplification and the newly synthesized product remains attached to the target, providing localized specific signals. In addition, the technology can be rapidly adapted to other clinical testing modalities, such as beads, tissues, plates, and microarrays. RCAT offers potential in developing accurate, quantitative, and standardized evaluation of individual immu-

Table 1. Signal amplification using RCAT compared with conventional methods.

	Events	Gated, ^a %	Median ^b	CV, %	Peak (events) ^c	MFI at peak	Median S/N ^d	Fold ^e
CD4 direct detection								
IgG-PE ^f direct control	3946	43.39	1	80	78	1.06		
CD4-PE	4458	49.11	243	4	85	250.29	183.17	
Antibody diluent, RCA	5002	55.36	1	79	69	1.01		
CD4-conjugate, RCA	4061	46.09	3219	6	37	4255.07	2090.70	11.41
CD4 indirect detection								
IgG-biotin (SA-Cy5) indirect control	6324	69.28	1	86	139	1.02		
CD4-biotin (SA-Cy5)	4644	51.26	39	4	110	40.68	30.27	
IgG-biotin, RCA (Cy5)	6085	68.13	1	77	149	1.01		
CD4-biotin, RCA (Cy5)	3406	38.33	1252	6	37	1553.84	948.60	31.34
CD28 indirect detection								
IgG-biotin, SA-Cy5 control	9027	93.32	3	52	76	3.30		
CD28-biotin, SA-Cy5	9344	97.26	29	49	65	43.32	13.12	
IgG-biotin, RCA	9152	97.27	4	55	69	5.04		
CD28-biotin, RCA	8975	98.85	89	58	47	723.40	143.53	10.94

^a Percentage of gated lymphocytes.

^b MFI values for gated lymphocytes.

^c Number of events in the peak with highest MFI values.

^d S/N, signal-to-noise ratio of median values.

^e Fold amplification based on signal-to-noise ratios.

^f PE, phycoerythrin; SA, streptavidin.

nologic responses, which has become increasingly important with the advancement of several immunotherapeutic interventions to clinical trials in recent years.

We acknowledge Dave Riches, Mehul Patel, Edward Zelazny, Dr. Osama Alsmadi, and Dr. Vanessa Wheeler for their contributions.

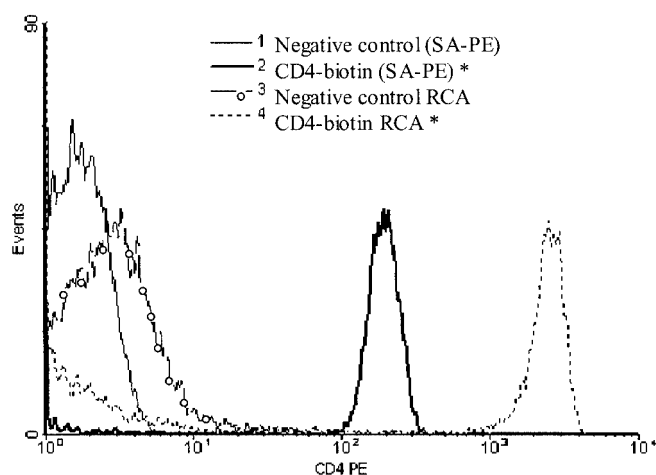


Fig. 1. Comparative flow cytometric analysis of CD4 expression in PBMCs.

*, the photomultiplier tube setting was reduced for these test samples (compared with negative controls) to get the complete peaks on scale because the RCA signals were above the fourth log in intensity. Maximum number of events for the CD4-biotin [streptavidin-phycoerythrin (SA-PE)] usually occurs at a signal intensity of 10^3 .

References

1. Wiltshire S, O'Malley S, Lambert J, Kukanskis K, Edgar D, Kingsmore SF, et al. Detection of multiple allergen-specific IgEs on microarrays by immunoassay with rolling circle amplification. *Clin Chem* 2000;46:1990-3.
2. Schweitzer B, Wiltshire S, Lambert J, O'Malley S, Kukanskis K, Zhu Z, et al. Inaugural article: immunoassays with rolling circle DNA amplification: a versatile platform for ultrasensitive antigen detection. *Proc Natl Acad Sci U S A* 2000;97:10113-9.
3. Schweitzer B, Kingsmore S. Combining nucleic acid amplification and detection. *Curr Opin Biotechnol* 2001;12:21-7.
4. Gusev Y, Sparkowski J, Raghunathan A, Ferguson H Jr, Montano J, Bogdan N, et al. Rolling circle amplification: a new approach to increase sensitivity for immunohistochemistry and flow cytometry. *Am J Pathol* 2001;159:63-9.
5. Davis KA, Lin Y, Abrams B, Jayasena SD. Staining of cell surface human CD4 with 2'-F-pyrimidine-containing RNA aptamers for flow cytometry. *Nucleic Acids Res* 1998;26:3915-24.
6. Lenkei R, Andersson B. Determination of the antibody binding capacity of lymphocyte membrane antigens by flow cytometry in 58 blood donors. *J Immunol Methods* 1995;183:267-77.

Rolling Circle Amplification Improves Sensitivity in Multiplex Immunoassays on Microspheres, Michael C. Mullenix,* Ramou Sivakamasundari, William J. Feaver, R. Murli Krishna, Martin P. Sorette, Hirock J. Datta, David M. Morosan, and Steven P. Piccoli (Molecular Staging Inc., 300 George St., New Haven, CT 06511; * author for correspondence: fax 203-772-5276, e-mail mikem@molecularstaging.com)

Microspheres are a proven solid-phase format for development of assays used in both research and clinical diagnostics. They can be manufactured in homogeneous batches incorporating very precise quantities of fluores-

cent dyes. Different amounts of fluorescent dyes in individual microspheres are easily distinguished by a flow cytometer. Quantitative immunoassays can be performed on the surface of the bead by use of a second fluorophore-based detection system compatible with the flow cytometer. The different bead types can be used to prepare separate immunoassays, which can later be combined in a multiplexed assay capable of simultaneously detecting multiple analytes (1, 2). The cytometric bead array products from Becton Dickinson and the Luminex bead format assays manufactured by Upstate Biotechnologies, Bio-Rad, and Biosource take advantage of this approach to multiplexing. These multiplex immunoassays are built on beads distinguishable in flow cytometers by their different fluorophore content. There are, however, numerous examples where important biological markers for cancer, infectious disease, or biochemical processes are present in body fluids or tissues at concentrations too low to be detected by conventional immunoassays (3–5). With these needs in mind, we have adapted the Rolling Circle Amplification (RCA) reporter system (6–8) to the detection of protein antigens (immunoRCA). In immunoRCA, the 5' end of an RCA primer is attached to an antibody. Thus, in the presence of circular DNA, Phi29 DNA polymerase, and nucleotides, the rolling circle reaction produces a concatamer of the complement of the circular DNA sequence that extends from the end of the original primer remaining attached to the antibody. The amplified DNA can be detected by hybridization of complementary oligonucleotide probes or by antibodies specific for nucleotide analogs incorporated during the RCA reaction.

RCA is well suited to flow cytometry bead assay formats because the amplification product remains tethered to the target molecules captured by the microsphere and does not interfere with the intrinsic fluorescence of the microsphere. We set out to demonstrate that immunoRCA offers improved sensitivity while maintaining the multiplexing capability of flow cytometer-based microsphere immunoassays.

ImmunoRCA was previously shown to improve sensitivity in several immunoassay formats, including enzyme-amplified assays in microtiter plates and on microspheres (6). We have also demonstrated that immunoRCA, by increasing sensitivity, enabled the use of microarrays for allergen-specific IgE detection (7, 8). Without RCA, microarray format immunoassays were unable to provide the detection limit achieved in commercially available allergen-specific IgE immunoassays. The allergen-specific IgE microarray assay demonstrated the compatibility of immunoRCA with multiplexed assays utilizing spatial separation to differentiate the separate immunoassays carried out simultaneously on the same sample. The spatial separation on microarrays is in principle the same approach taken in multiplexed microsphere immunoassays. In the present study, immunoRCA was applied to monoplex and multiplex cytometric bead immunoassays purchased from Bio-Rad, Upstate Biotechnology, Becton Dickinson, and Biosource International.

All non-immunoRCA assays used the manufacturers' provided procedures.

In each of the commercial immunoassays, a sandwich immune complex is formed between the capture antibody on the bead, the analyte, and the biotinylated detector antibody. In all cases, the bound biotinylated antibody is detected by use of a streptavidin-phycoerythrin (SA-PE) conjugate. In immunoRCA assays, the SA-PE is replaced by an anti-biotin monoclonal antibody (Jackson ImmunoResearch) conjugated to a 35mer oligonucleotide RCA primer as described previously (6). Before use in the assay, the anti-biotin antibody RCA primer conjugate was hybridized to circular DNA in a solution of phosphate-buffered saline (PBS) containing 0.5 mL/L Tween 20 and 2 mmol/L EDTA for 30 min at 37 °C. After the sandwich immune complex formed, the microspheres were washed once in 200 μ L of PBS containing 0.5 mL/L Tween 20 on a 96-well vacuum filter plate, resuspended in the anti-biotin RCA primer conjugate preannealed to circle, and then incubated for 30 min at room temperature. After incubation, the microspheres were washed once in PBS containing 0.5 mL/L Tween 20 and once in 200 mmol/L potassium glutamate, 35 mmol/L HEPES (pH 7.5), 20 mmol/L magnesium acetate, and 70 mg/L bovine serum albumin. The RCA reaction with biotin incorporation was carried out for 1 h at 31 °C after the microspheres were resuspended in 200 mmol/L potassium glutamate, 35 mmol/L HEPES (pH 7.5), 20 mmol/L magnesium acetate, 70 mg/L bovine serum albumin, 100 μ mol/L dATP, 100 μ mol/L dCTP, 100 μ mol/L dGTP, 22.5 μ mol/L dTTP, 2.5 μ mol/L biotin-dUTP, 7 mmol/L dithiothreitol, and 1 U/ μ L Phi29 polymerase. After the RCA reaction, the beads were washed twice with PBS containing 0.5 mL/L Tween 20, and the incorporated biotin was detected by resuspending the beads in 1.5 mg/L SA-PE in PBS containing 0.5 mL/L Tween 20 and incubating at 37 °C for 30 min. Finally the beads were washed twice in PBS containing 0.5 mL/L Tween 20 and resuspended in PBS containing 0.5 mL/L Tween 20. The fluorescence intensity of the microspheres was quantified using a Luminex 100 instrument.

ImmunoRCA was applied to multiplexed cytokine microsphere immunoassays manufactured by Upstate Biotechnology and Biosource International. The Upstate Biotechnology assay was designed to detect five human cytokines, including interleukin (IL)-2, IL-4, tumor necrosis factor- α (TNF α), granulocyte-macrophage colony-stimulating factor (GM-CSF), and interferon- γ (IFN γ). The Biosource International assay was designed to detect 10 human cytokines, including the 5 above and IL-1 β , IL-5, IL-6, IL-8, and IL-10. To determine the magnitude of the improvement provided by immunoRCA, serial dilutions of cytokines were tested in both assays with and without the addition of immunoRCA. The minimum detection limit for each cytokine assay with and without immunoRCA was interpolated from calibration curves (Fig. 1). The minimum detection limits for the immunoRCA and standard assays were determined for both cytokine assays, and the fold improvement in detection limit was

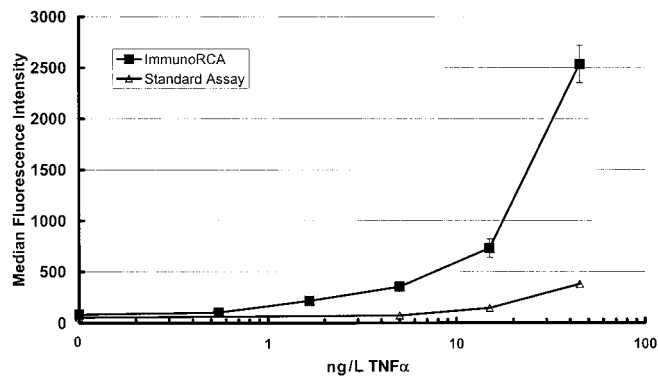


Fig. 1. Improved detection limit of TNF α microsphere immunoassay with immunoRCA.

Calibration curves representing the five cytokines detected in the Upstate Biotechnology cytokine immunoassay were run with and without immunoRCA. The TNF α calibration curve is provided to demonstrate the improvement in detection limit provided by immunoRCA. Each data point represents the mean of three replicates.

calculated (Table 1). The minimum detection limit for this study was defined as the cytokine concentration providing fluorescence equivalent to 2 SD above the fluorescence at zero cytokine. The CV (%) observed at the first cytokine concentration tested above the minimum detection limit is provided as a measure of the variability of the assay near the minimum detection limit. The fold improvement in detection limit provided by RCA varied considerably, ranging from no improvement in two cytokine assays to 100-fold. Two potential sources of the differences in fold improvement provided by immunoRCA are the affinity of

the antibody pairs in the immune complex and the possibility that the immune complex formed by some antibody pairs may be sensitive to the RCA reaction buffer conditions. The mean fold improvement observed for the 15 individual cytokine assays examined in the two multiplex assays was 33-fold.

Similar improvements in the detection limit were achieved in the Luminex format assays manufactured by Bio-Rad, as well as in assays designed for use in conventional flow cytometers, such as the cytometric bead array assays from Becton Dickinson (unpublished data). Typical intraassay CVs recently were 10–20% in multiplex immunoRCA microsphere assays. The compatibility of immunoRCA for use with serum, plasma, and tissue culture supernatants has also been established (unpublished data).

To address the effect of immunoRCA on multiplex assay specificity, single cytokines were tested in the Upstate Biotechnology multiplex assay (data not shown). No cross-reactivity between cytokines was observed up to single cytokine concentrations of 100 ng/L. In addition, detection of multiple cytokines did not alter the detection limits for individual cytokine assays in the Upstate Biotechnology multiplex assay. ImmunoRCA decreased the dynamic range in some assays. In all cases to date, the dynamic range of the RCA assay has overlapped the dynamic range of non-RCA assays. If increased dynamic range is required, we suggest that researchers run the non-RCA assay in parallel to extend the dynamic range.

The results indicate that immunoRCA has the potential to provide sensitivity improvements in flow cytometry-based microsphere immunoassays. Many cytokines are

Table 1. Improvement in minimum detection limit^a by immunoRCA in microsphere immunoassays.

Cytokine	Standard assay		ImmunoRCA Assay		Improvement in detection limit, fold
	MDL, ^b ng/L	CV, ^c %	MDL, ng/L	CV, ^c %	
Upstate Biotechnology Assay					
IL-2	0.8	28 (5.0)	0.18	8.6 (0.55)	4.4
IL-4	0.18	16 (5.0)	0.19	4.6 (0.55)	None
TNF α	8	4.1 (15.0)	0.15	12 (0.55)	53.3
GM-CSF	0.78	16 (5.0)	0.56	12 (1.66)	1.4
IFN γ	10.2	20 (15.0)	0.9	8.1 (1.66)	11.3
Biosource International Assay					
IL-1 β	9.38	3.3 (23.5)	4.69	8.6 (9.38)	2.0
IL-2	11.08	5.6 (22.2)	0.11	9.6 (0.22)	100.7
IL-4	5.00	6.5 (10.0)	0.05	5.2 (0.10)	100.0
IL-5	0.78	7.0 (1.6)	0.08	8.3 (0.15)	9.8
IL-6	2.59	9.4 (5.2)	2.59	3.0 (5.18)	None
IL-8	0.78	2.0 (1.6)	0.01	15 (0.02)	78.0
IL-10	0.80	1.4 (1.6)	0.08	27 (0.16)	10.0
TNF α	4.38	8.7 (8.8)	0.44	6.9 (0.87)	9.9
GM-CSF	8.70	10 (17.5)	0.09	14 (0.17)	96.6
IFN γ	1.52	7.3 (7.6)	0.08	14 (0.15)	19

^a Minimum detection limits were determined at 2 SD above the 0 ng/L background fluorescence for each cytokine.

^b MDL, minimum detection limit.

^c The CV is provided for the first cytokine concentration tested above the minimum detection limit. The first cytokine concentration tested above the minimum detection limit is provided in parentheses.

likely to have biological activity at concentrations well below the detection limits of commercially available immunoassays. The improved detection limits and compatibility with multiplexed assays will enable immunoRCA-amplified assays to potentially redefine cytokine biology. The technology could enable scientists to study complex mixtures of cytokines at lower concentrations than previously possible. Additionally, the added sensitivity could allow dilution of samples, thereby increasing the number of experiments that could be completed with a single sample. Sample dilution may also allow investigators to extend timelines for critical samples in existing studies.

Clinical diagnostics could also benefit from immunoRCA addition to flow cytometry-based microsphere immunoassays. ImmunoRCA will improve existing assays by lowering detection limits for critical targets such as blood-borne viruses and other pathogens. Other immunoassay amplification techniques, such as immuno-PCR or chemiluminescence, are not compatible with flow cytometry-based microsphere immunoassays because the amplification product is released into the supernatant. Immuno-PCR techniques would also break up the immune complex during thermocycling. As with any amplification system, immunoRCA will add cost and complexity to assays. The added cost should be incremental to the immunoassay reagent set. The impact of added complexity may be offset by the increased sensitivity. An added advantage with microsphere-based assays is that custom assay combinations can be assembled as needed by the physician. Compatibility with multiplex assays ensures that immunoRCA assays will maintain this degree of flexibility.

We would like to acknowledge David Riches for technical expertise in the manufacture of the protein-DNA conjugates.

References

1. Carson RT, Vignali DAA. Simultaneous quantitation of 15 cytokines using a multiplexed flow cytometric assay. *J Immunol Methods* 2000;227:41-52.
2. McHugh T. M. Flow microsphere immunoassay for the quantitative and simultaneous detection of multiple soluble analytes. *Methods Cell Biol* 1994;42:575-95.
3. Saito K, Kobayashi D, Sasaki M, Araake H, Kida T, Yagihashi A, et al. Detection of human serum tumor necrosis factor- α in healthy donors, using a highly sensitive immuno-PCR assay. *Clin Chem* 1999;45:665-9.
4. O'Connor E, Roberts EM, Davies JD. Amplification of cytokine-specific ELISAs increases the limit of detection to 5-20 picograms per milliliter. *J Immunol Methods* 1999;229:155-60.
5. Kimura H, Suzui M, Nagao F, Matsumoto K. Highly sensitive determination of plasma cytokines by time resolved fluoroimmunoassay: effect of bicycle exercise on plasma level of interleukin 1 α (IL-1 α), tumor necrosis factor α (TNF α), and interferon γ (IFN γ). *Anal Sci* 2001;17:593-7.
6. Schweitzer B, Wiltshire S, Lambert J, O'Malley S, Kukanskis K, Zhu Z, et al. Immunoassays with rolling circle amplification: a versatile platform for ultrasensitive antigen detection. *Proc Natl Acad Sci U S A* 2000;97:10113-9.
7. Wiltshire S, O'Malley S, Lambert J, Kukanskis K, Edgar D, Kingsmore S, et al. Detection of multiple allergen-specific IgEs on microarrays by immunoassay with rolling circle amplification. *Clin Chem* 2000;46:1990-3.
8. Mullen M, Wiltshire S, Shao W, Kitos G, Schweitzer B. Allergen-specific IgE detection on microarrays using rolling circle amplification: correlation with in vitro assays for serum IgE. *Clin Chem* 2001;47:1926-9.

Molecular Monitoring of Acute Promyelocytic Leukemia by DzyNA Reverse Transcription-PCR, Tanya L. Applegate,^{1*} Harry J. Iland,² Elisa Mokany,¹ and Alison V. Todd¹ (¹ Johnson & Johnson Research Pty Limited, Australian Technology Park, Eveleigh NSW 1430, Australia; ² Kanematsu Laboratories, Royal Prince Alfred Hospital, Camperdown, Sydney NSW 2050, Australia; * address correspondence to this author at: Biomedical Bldg., Level 4, 1 Central Ave., Australian Technology Park, Eveleigh NSW 1430, Australia; fax 61-2-83965811, e-mail tapplega@medau.jnj.com)

Acute promyelocytic leukemia (APL) is caused by inhibition of apoptosis and a block in myeloid differentiation resulting from a translocation invariably involving the retinoic acid α (*RAR α*) gene (1, 2). Ninety percent of breakpoints lie within intron 3 or 6 of the *PML* gene, producing fusion transcripts of the S-type (exon 3 *PML*/exon 3 *RAR α*) or L-type (exon 6 *PML*/exon 3 *RAR α*) isoform. The remaining patients have V-type transcripts, which vary in length depending on where the breakpoint lies within exon 6 of the *PML* gene. Although a combination of all-*trans*-retinoic acid (ATRA) differentiation therapy and chemotherapy successfully induces remission in the majority of patients harboring the *PML/RAR α* transcript, approximately one-third of these patients relapse (3). Patient survival rates are improved by initiating salvage therapy at molecular relapse rather than waiting for overt hematologic relapse (4, 5). Recent preliminary results suggest that the predictive power of molecular monitoring may be improved by the application of new quantitative methods to patient management (6, 7). This report provides the most recent patient results obtained with the single-tube DzyNA reverse transcription-PCR (RT-PCR) assay recently developed in our laboratory for diagnosing and monitoring APL (8).

DzyNA RT-PCR assays for quantification of *PML/RAR α* transcripts and endogenous *BCR* control transcripts were used to analyze total RNA from patients with APL. Specimens were analyzed with the investigator blinded to the patients' clinical histories. Primers, substrate, and reaction conditions for DzyNA RT-PCR and confirmatory two-step nested qualitative RT-PCR were as described previously (8). The *PML/RAR α* primers amplify all L-type, and most V-type, transcripts. *PML/RAR α* concentrations were normalized by use of *BCR* concentrations, thus controlling for variations in RNA integrity from clinical specimens. Quantitative data were expressed as ng-equivalents of the total NB4 RNA. Relative transcript amounts were expressed as a percentage ratio of disease transcripts to control transcripts (RDC %) calculated by the following equation:

$$\text{RDC}\% = 100\% \times \frac{\text{NB4 ng-equivalents of PML/RAR}\alpha \text{ per 50 ng of patient RNA}}{\text{NB4 ng-equivalents of BCR per 50 ng of patient RNA}}$$

The criteria for inclusion and exclusion of data were as described previously (8).

RNA was analyzed from a cohort of 39 patients whose bone marrow was collected at the time of diagnosis of APL. *PML/RAR α* transcripts were detected in all patients' RNA, confirming the clinical diagnosis of APL, and there was complete concordance between DzyNA RT-PCR and nested RT-PCR. The overall average RDC was 185% (range, 16–2342%). This wide range provides an explanation, in addition to technical reasons, for the disparity in reports of detection limits determined by dilutions of patients' RNA. There appeared to be higher amounts of transcripts in patients with V-type ($n = 4$; range, 258–2342%; mean, 998%) than in patients with L-type ($n = 35$ patients; range, 16–269%; mean, 94%). This is the first report of quantification of V-type transcripts, and although the number of data points is too small for statistical significance, these results are interesting in light of studies suggesting that V-form patients exhibit a worse prognosis than patients with other isoforms (9). Ongoing studies aim to determine whether transcript concentrations at diagnosis are of prognostic significance.

DzyNA RT-PCR was used to analyze serial samples from three APL patients. These patients are enrolled in the APLM3 Clinical Trial currently being conducted by the Australasian Leukaemia and Lymphoma Group. This international multicenter trial is studying patients receiving ATRA combined with idarubicin. Bone marrow specimens were analyzed prospectively at the treating hospitals by standard nested RT-PCR (data not shown) and retrospectively in our laboratory by DzyNA RT-PCR and nested RT-PCR. Fig. 1 shows the results of molecular monitoring of patients A, B, and C, quantifying the expression of *PML/RAR α* relative to *BCR* in panels A, B and C respectively.

Trial patient A had above-average amounts of the L-form *PML/RAR α* mRNA (RDC = 196%) at diagnosis (Fig. 1A, points 1 and 2) and was treated with ATRA and idarubicin. Although normal bone marrow morphology and cytogenetics indicated hematologic remission (point 3), prospective nested RT-PCR detected fusion transcripts, and the patient was given a second course of idarubicin. Fusion transcripts were still detectable by nested RT-PCR after idarubicin therapy (point 4), and intermittent ATRA therapy was initiated shortly thereafter. Retrospective DzyNA RT-PCR and nested RT-PCR confirmed the presence of *PML/RAR α* mRNA during this period and showed that the amounts had decreased at a constant rate over 37 weeks (points 2–5). Transcripts were still detectable by DzyNA RT-PCR at the conclusion of consolidation treatment (point 5), but were undetectable 3 months later (point 6). All subsequent samples (points 7–9) were negative for *PML/RAR α* transcripts by all protocols.

Trial patient B presented with low amounts of L-type *PML/RAR α* mRNA (RDC = 25%; Fig. 1B, point 1). The patient was treated with ATRA (point 2), and fusion

transcripts were undetectable by all protocols within 11 weeks (point 4). The patient remained in clinical remission for 8 months, during which fusion transcript values were either undetectable or low by DzyNA RT-PCR (points 4–7). The patient eventually relapsed (point 8) with both hematologic and molecular symptoms. ATRA treatment was offered but refused for 2.5 months (points 8 and 9). The patient then agreed to 1 month of ATRA treatment, and *PML/RAR α* transcripts became undetectable (point 10). Consolidation therapy was refused, and the next samples showed a reemergence of *PML/RAR α* transcripts (points 11–12), which was followed by frank hematologic relapse (point 13). Offers of ATRA treatment were refused during this period (points 11–13), but the patient again consented to 1 month of ATRA therapy, which led to clearance of the *PML/RAR α* mRNA within 5 weeks (point 14). Stem cells were harvested (point 15),

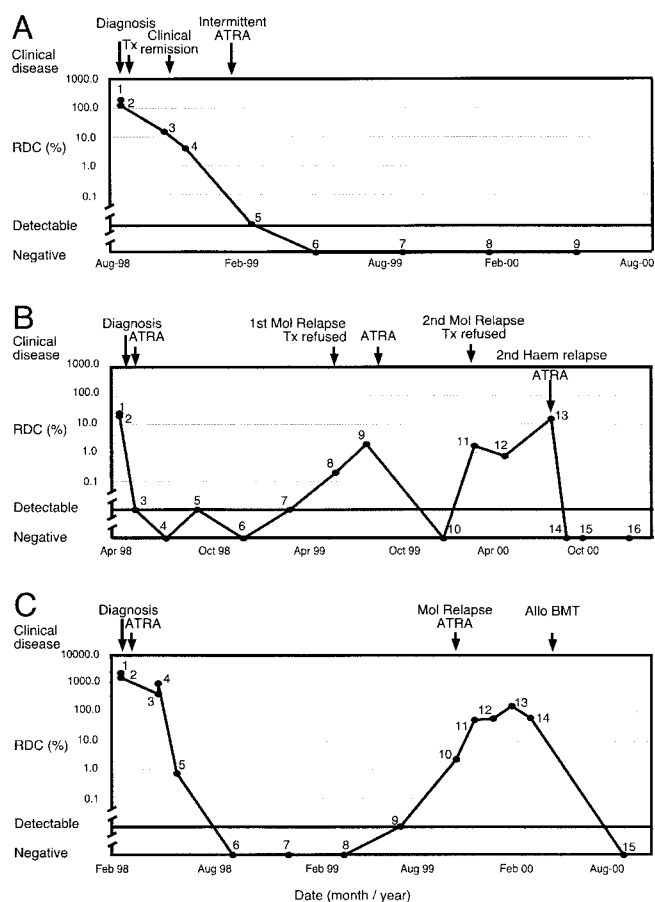


Fig. 1. Molecular monitoring of *PML/RAR α* transcripts relative to *BCR* for APL Trial patients A, B, and C (panels A–C, respectively).

The expression of *PML/RAR α* and *BCR* was estimated from calibration curves, and the RDC (%) was calculated and plotted against time. Samples that could not be quantified were classified as either detectable (samples that were positive by both DzyNA RT-PCR and nested PCR) or negative (samples that were negative by both DzyNA RT-PCR and nested PCR). Result points are numbered for clarification during the discussion in the text. The disease stages and times of administration of therapy (Tx) are shown above each graph. Mol, molecular; Haem, hematologic; BMT, bone marrow transplant.

shown to be negative for disease by nested RT-PCR, and then transplanted back into the patient (point 16).

Trial patient C presented with very high amounts of V-type *PML/RAR α* mRNA (RDC = 2342%; Fig. 1C, point 1). The patient received ATRA therapy and achieved hematologic remission in 12 weeks (point 5). At this time, *PML/RAR α* transcripts were still detectable by nested RT-PCR, but subsequent analysis by DzyNA RT-PCR showed that expression was very low. The fusion transcript became undetectable by both protocols 12 weeks later (point 6) and remained undetectable for 6 months (points 7 and 8). DzyNA analysis detected very low amounts of fusion transcripts (point 9), which increased in the subsequent sample (point 10). These fusion transcripts had been detected prospectively by nested RT-PCR in this sample (point 10), and the patient was offered ATRA despite the absence of evidence of hematologic relapse. Despite ATRA therapy, fusion transcripts remained high for the next 17 weeks (points 11–14). This patient then received an allogeneic bone marrow transplant, which was successful in inducing hematologic and molecular remission (point 15).

In the three cases above, the relative *PML/RAR α* amounts determined by DzyNA RT-PCR correlated well with the clinical history. The assay detected increases in transcript concentrations 3–6 months before morphologic or cytologic symptoms of relapse. Although the literature reports that most patients achieve clinical remission within 1–2 months of ATRA therapy (10), the rates of clearance of fusion transcripts appear more variable. Patient A took 6 weeks to achieve clinical remission, but it was >9 months before fusion transcripts were undetectable. In contrast, patient B demonstrated rapid clearance of *PML/RAR α* transcripts in as little as 4.5 weeks after treatment. Patient C initially achieved hematologic remission after initial ATRA therapy despite the very high leukemic burden. However, despite prompt re-initiation of therapy on detection of fusion transcripts, the amounts of fusion transcript remained high, indicating resistance to ATRA. Persistence of fusion transcripts should aid the identification of “nonresponders” who would benefit from alternative therapy. In patient B, fusion transcripts were detected at very low amounts in a sample (point 5) between two remission samples, which were negative for fusion transcripts. Ongoing studies will determine whether these “interruptions” of molecular remission are of prognostic significance and/or identify patients who have not completely cleared the malignant clone and may be at greater risk of relapse.

Studies monitoring APL patients by DzyNA RT-PCR will continue to assess the prognostic significance of several factors highlighted by the examples in this study. Potential factors influencing outcome may include the fusion transcript isoform, the relative amounts at diagnosis, and rates of clearance and accumulation, as well as intermittent detection of transcripts during clinical remis-

sion. Continuing studies aim to further demonstrate the potential for use of quantitative molecular monitoring to facilitate early prediction of imminent relapse and to investigate the impact on disease-free survival of efforts to optimize the timing of administration of salvage therapy based on molecular information.

We acknowledge Li Chong, Shane Supple, Juliet Ayling, Francisca Springall, and Albert Catalano from the Kanematsu Laboratories for assistance in clinical specimen collection and collation. We are very grateful to the Australasian Leukaemia and Lymphoma Group clinicians for allowing access to clinical specimens and patient histories.

References

1. Piazza F, Gurrieri C, Pandolfi PP. The theory of APL. *Oncogene* 2001;20:7216–22.
2. Lin RJ, Sternsdorf T, Tini M, Evans RM. Transcriptional regulation in acute promyelocytic leukemia. *Oncogene* 2001;20:7204–15.
3. Degos L, Wang ZY. All-trans-retinoic acid in acute promyelocytic leukemia. *Oncogene* 2001;20:7140–5.
4. Lo Coco F, Diverio D, Avvisati G, Petti MC, Meloni G, Pogliani EM, et al. Therapy of molecular relapse in acute promyelocytic leukemia. *Blood* 1999;94:2225–9.
5. Lo Coco F, Diverio D, Falini B, Biondi A, Nervi C, Pelicci PG. Genetic diagnosis and molecular monitoring in the management of acute promyelocytic leukemia. *Blood* 1999;94:12–22.
6. Tobal K, Moore H, Macheta M, Yin JA. Monitoring minimal residual disease and predicting relapse in APL by quantitating *PML-RAR α* transcripts with a sensitive competitive RT-PCR method. *Leukemia* 2001;15:1060–5.
7. Slack JL, Bi W, Livak KJ, Beaubier N, Yu M, Clark M, et al. Pre-clinical validation of a novel, highly sensitive assay to detect *PML-RAR α* mRNA using real-time reverse-transcription polymerase chain reaction. *J Mol Diagn* 2001;3:141–9.
8. Applegate TL, Iland HJ, Mokany E, Todd AV. Diagnosis and molecular monitoring of acute promyelocytic leukemia using DzyNA reverse transcription-PCR to quantify *PML/RAR α* fusion transcripts. *Clin Chem* 2002;48:1338–43.
9. Slack JL, Willman CL, Andersen JW, Li YP, Viswanatha DS, Bloomfield CD, et al. Molecular analysis and clinical outcome of adult APL patients with the type V *PML-RAR α* isoform: results from intergroup protocol 0129. *Blood* 2000;95:398–403.
10. Fenaux P, Chomienne C, Degos L. Treatment of acute promyelocytic leukaemia. *Best Pract Res Clin Haematol* 2001;14:153–74.

Homogeneous Assay for Tyrosine Kinase: Use of Bacteriophage Antibody Conjugates in an Assay for p56^{lck} Kinase, Jay Patel, Christopher J. Stanley, and Stuart M. Wilson (Microsens Biotechnologies, London Bioscience Innovation Centre, 2 Royal College Street, London NW1 0TU, England; * author for correspondence: fax 44-20-7691-2036, e-mail jay.patel@microsens.co.uk)

Protein kinases play a critical role in almost every cellular regulatory process and have been identified as key players in diseases such as cancer and immune syndromes (1). For this reason, there has been substantial interest in the development of assays for protein kinases for use as both diagnostics and drug discovery tools (2). Although several assays exist for kinases, the most commonly used involve monitoring transfer of the γ -phosphoryl group from [γ -³²P]ATP to a peptide substrate (3). These assays

are cumbersome to implement because the unreacted [γ - 32 P]ATP needs to be separated from the phosphorylated peptide by use of separation techniques such as gel electrophoresis.

In drug discovery programs, fluorescence resonance energy transfer (FRET) kinase assays are becoming increasingly popular because they are homogeneous, making them relatively easy to automate (4). In typical FRET assays, the anti-phosphotyrosine antibody and the substrate peptide are labeled with "donor" and "acceptor" fluorophores. On phosphorylation of the peptide, the anti-phosphotyrosine antibody binds to the peptide, and the two fluorophores are brought in close proximity to each other. Excitation of the acceptor fluorophore leads to energy transfer to the donor molecule, which emits fluorescence. The principal disadvantage of FRET-based assays is that they are difficult to configure because the two fluorophores need to be within a closely defined distance of each other.

The Dual Phage technology is a new ultrasensitive biological amplification system of broad applicability that uses bacteriophages as biological amplification tools (5). The Dual Phage technology uses two types of bacteriophages that encode two selectable markers. The phages are labeled with an interacting pair, e.g., a receptor/agonist or enzyme/substrate combination. When the interaction takes place, the two phages become spatially linked in the complex and can then infect the same bacterial host cell (the "indicator organism"), thus conferring resistance to both selective agents. This dual infection event is markedly enhanced by the close proximity of the two phages in the complex. When the two selective agents are added to the medium, only the doubly infected indicator organisms survive, and the signal monitored is the growth of these cells.

Several other biological amplification methods have also been devised for the study of molecular interactions. For example, immuno-PCR is a sensitive technique that detects antigens by binding a DNA-tagged antibody to the antigen, amplifying the DNA by PCR, and then detecting the DNA product (6). In immunodetection amplified by T7 RNA polymerase, a double-stranded oligonucleotide containing the T7 promoter is conjugated to an antibody, and then T7 RNA polymerase is used to amplify RNA from the double-stranded oligonucleotides coupled to the antibody in the antibody-antigen complex (7).

Using a version of the Dual Phage technology adapted for enzyme assays (Fig. 1A), we have developed a highly sensitive homogeneous assay for lck kinase (p56^{lck}). p56^{lck} kinase is a membrane-associated nonreceptor tyrosine kinase that is found exclusively in natural killer (TK) cells and T cells (8) that play a critical role in T-cell development and activation. The p56^{lck} kinase is localized to a site on the genome that frequently contains chromosomal abnormalities in lymphomas and neuroblastomas (9). In light of these observations, inhibitors for p56^{lck} kinase could have important applications in the treatment of autoimmune and cancer disease.

The kinase substrate peptide (RRLIEDAEYAARG-biotin; Pierce) was coupled to streptavidin-derivatized M13 (encoding for ampicillin resistance) by standard biotin-streptavidin conjugation techniques (10). Biotinylated anti-phosphotyrosine antibody (Sigma) was coupled to a streptavidin-derivatized M13 bacteriophage encoding for chloramphenicol resistance. These phage conjugates were purified on an affinity column containing anti-M13 antibody (Sigma) bound to agarose. Using the Sigma protein tyrosine kinase assay reagent set (nonradioactive), we determined that each phage carried ~10–100 ligands.

As illustrated in Fig. 1B, the Dual Phage technology has been successfully applied to the development of a homo-

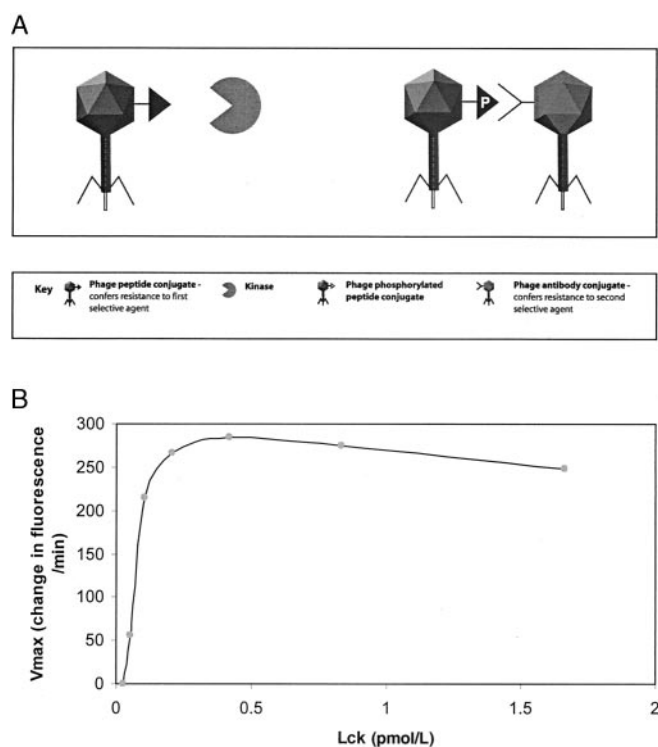


Fig. 1. Schematic of the dual phage kinase assay (A) and lck kinase dilution curve (B).

(A), synthetic peptide substrate is attached to a phage carrying resistance to chloramphenicol (phage C). The second phage is labeled with an anti-phosphotyrosine antibody and codes for ampicillin resistance (phage A). In the presence of kinase and ATP, the peptide substrate on phage C is phosphorylated, and the anti-phosphotyrosine antibody on phage A binds to the newly generated phosphate group, forming the dual-phage complex. Addition of *E. coli* (the indicator organism) leads to rapid dual infection of the bacterial cells by phages A and C. The growth of viable *E. coli* cells (in the presence of chloramphenicol and ampicillin) is monitored in real time by use of a redox indicator. (B), serial dilutions of p56^{lck} kinase (Upstate) were prepared in kinase buffer [10 g/L bovine serum albumin, 20 mmol/L HEPES (pH 7.4), 10 mmol/L MgCl₂, 100 μ mol/L CaCl₂]. A 10- μ L aliquot of each dilution was placed in a flat-bottomed black microtiter plate together with 10 μ mol/L ATP; 10 μ L of phage C-peptide substrate (10^5 virions) conjugate was then incubated with the kinase for 30 min at room temperature. Phage A-anti-phosphotyrosine antibody conjugate (10 μ L, containing 10^5 virions) was then added to the reaction and left to incubate for 30 min at room temperature. A 200- μ L aliquot of a log-phase culture of *E. coli* ($\sim 5 \times 10^7$ cells) was added and incubated at 37 °C for 5 min; 5 μ L (5 μ mol/L) of C₁₂-resazurin (Molecular Probes) and 10 μ L of ampicillin and chloramphenicol (10 μ g of each) were added to the reactions. The plate was covered with a transparent "breathable" plate seal (Nalge Nunc), and the change in fluorescence (excitation/emission at 530/590 nm) per min was recorded over a period of 4 h (V_{max}) on a plate reader.

geneous microtiter plate-based assay for p56^{lck} kinase. In the assay incubation, the optimum number of each phage was 10⁵ virions. Previous optimization experiments had shown that use of a lower phage concentration decreased the signal and increased the detection time, whereas use of a higher concentration led to an increase in the background signal. At the optimum phage concentration, the signal-to-background ratio of the Dual Phage technology was >10:1. In replicate p56^{lck} kinase assays, the CV was 5.1% (n = 10).

We conclude that the Dual Phage lck kinase assay has a lower detection limit (0.05 pmol/L lck kinase) lower than other homogeneous lck kinase assays. For example, the Packard HTRF lck assay has a lower detection limit of 2 pmol/L (11). The homogeneous nature of the Dual Phage assay makes it ideally suited to both automation and miniaturization. The labeled phages and the indicator organism are extremely robust (no loss of activity has been seen in phage conjugates and freeze-dried *Escherichia coli* stored at 4 °C over a period of 6 months) and can be readily prepared by standard techniques. The flexibility of the Dual Phage technology suggests that the kinase assay can be implemented in many formats, such as microplate, magnetic particle, or microfluidics systems. The output signal from the indicator organism can be adapted to match existing instruments such as fluorometers, colorimeters, or luminometers. Potential uses for this kinase assay include discovery of kinase inhibitors in high-throughput screening campaigns and use in clinical diagnostic assays.

References

- Hunter T. Protein kinases and phosphatases: the yin and yang of protein phosphorylation and signalling. *Cell* 1995;80:225–36.
- Williams DM, Cole PA. Kinase chips hit the proteomics era. *Trends Biochem Sci* 2001;26:271–3.
- Casnellie JE. Assay of protein kinases using peptides with basic residues for phosphocellulose binding. *Methods Enzymol* 1991;200:115–20.
- Kolb AJ, Kaplita PV, Hayes DJ, Park YW, Pernell C, Major JS, et al. Tyrosine kinase assays adapted to homogeneous time-resolved fluorescence. *Drug Discov Today* 1998;3:333–42.
- Wilson SM, inventor. Analytical method using multiple virus labelling. World patent WO9963348A1, 1999.
- Sano T, Smith CL, Cantor CR. Immuno-PCR: very sensitive antigen detection by means of specific antibody-DNA conjugates. *Science* 1992;258:120–2.
- Zhang HT, Kacharina JE, Miyashiro K, Greene MI, Eberwine J. Protein quantification from complex protein mixtures using a proteomics methodology with single-cell resolution. *Proc Natl Acad Sci U S A* 2001;8:98:5497–502.
- Veillette A, Abraham N, Caron L, Davidson D. The lymphocyte-specific tyrosine protein kinase p56^{lck}. *Semin Immunol* 1991;3:143–52.
- Abraham KM, Levin SD, Marth JD, Forbush KA, Perlmutter RM. Thymic tumorigenesis induced by over expression of p56^{lck}. *Proc Natl Acad Sci U S A* 1991;1:88:3977–81.
- Hermanson GT, ed. *Bioconjugation techniques*. New York: Academic Press, 1996:570–91.
- Park YW. Development and miniaturization of an HTRF tyrosine kinase assay [Application Note]. Document No. AN4002-DSC. Meridian, CT: Packard Instrument Company, 1999.

Detection of Circulating Thyroid Cancer Cells by Reverse Transcription-PCR for Thyroid-stimulating Hormone Receptor and Thyroglobulin: The Importance of Primer Selection, Manjula K. Gupta,^{1*} Leslie Taguba,² Rosemary Arciaga,¹ Allan Siperstein,³ Charles Faiman,² Adi Mehta,² and S. Sethu K. Reddy² (Departments of ¹ Clinical Pathology, ² Endocrinology, and ³ General Surgery, The Cleveland Clinic Foundation, Cleveland, OH 44195; * address correspondence to this author at: Department of Clinical Pathology, L-30, The Cleveland Clinic Foundation, 9500 Euclid Ave., Cleveland, OH 44195; fax 216-445-9444, e-mail guptam@ccf.org)

Monitoring for thyroid cancer recurrence is routinely done through measurement of serum thyroglobulin (Tg) and ¹³¹I whole-body scanning (WBS) after total thyroidectomy and radioactive iodine ablation (1). Serum Tg has been a useful marker to detect residual or metastatic disease, but its limitations include interassay variability, insufficient sensitivity of some commercial assays, and the frequent presence of interfering anti-Tg antibodies in patient serum (2, 3). Although the ability of serum Tg to detect metastatic disease improves greatly after thyroid hormone withdrawal, hormone withdrawal produces symptomatic hypothyroidism and significant morbidity in many patients.

Sensitive detection of circulating cancer cells by reverse transcription-PCR (RT-PCR) of tumor-specific mRNA appears to be a useful adjunct in monitoring of some other malignancies (4, 5). RT-PCR has been used to detect thyroid cells in circulation by amplifying transcripts of the thyroid tissue-specific Tg gene (6–8), but Tg mRNA can be found normally in circulation (7, 8). Recently, real-time quantitative RT-PCR has been reported to detect small amounts of Tg mRNA in the blood of healthy individuals and to identify thyroid cancer patients with recurrent and residual disease (9–11). Furthermore, Savagner et al. (11) reported that the amount of a Tg mRNA alternative splicing variant closely correlated with the thyroid volume and thyroid-stimulating hormone (TSH) concentration.

Thyroid carcinomas contain functional TSH receptor (TSHR) (12, 13), and differentiated thyroid cancer micro-metastases have been detected by RT-PCR of TSHR and Tg mRNAs (14). TSHR has not been exploited to detect circulating cancer cells, and smaller TSHR transcripts have been detected in human lymphocytes (15).

We investigated the specificity of different PCR primer pairs in the amplification of TSHR and Tg mRNA signals in blood samples from healthy individuals and in thyroid cancer tissue. Selected primer pairs with specificity for thyroid tissue and no reactivity with normal peripheral blood mononuclear cells (PBMCs) were further tested to evaluate the potential for clinical utility on detection of circulating thyroid cells.

Four TSHR primer pairs were tested against a panel of normal PBMC RNA and thyroid cancer tissue RNA. One of these was designed to amplify a segment in exons 9 and 10, starting at nucleotide 873 and ending at nucleotide

1371 (TSHR-1; 498 bp). Two were designed to amplify segments in exon 10, spanning nucleotides 1365–1851 (TSHR-2; 486 bp) and 1813–2316 (TSHR-3; 503 bp). The fourth primer pair was targeted to amplify a segment spanning exons 6–9 (14), starting at nucleotide 555 and ending at nucleotide 767 (TSHR-4A; 212 bp). The primer sequences for TSHR were as follows:

TSHR-1: forward, 5'-TTTCTTACCCAAGCCACTGC-3'; reverse, 3'-GCTTATTCTCCTCACCAGCC-5'
 TSHR-2: forward, 5'-CATAGTTGCCTTCGTCATCG-3'; reverse, 3'-GCAAGGCCAAATCTCAGAAG-5'
 TSHR-3: forward, 5'-CCAGCCACTACAAACTGAA-CG-3'; reverse, 3'-CGTCTGCTGCTGTTATGTGA-5'
 TSHR-4: forward, 5'-GCTTTTCAGGGACTATGCAAT-GAA-3'; reverse, 3'-JAGAGTTTGGTACAGT-GACGGGAA-5'

For comparison we also tested three previously described (6, 7, 14) Tg primer pairs for specificity, all targeted to exons 1–5 and spanning nucleotides 99–447 (Tg-1; 348 bp), 112–519 (Tg-2; 407 bp), and 33–562 (Tg-3; 529 bp). The primer sequences were as follows:

Tg-1: forward, 5'-TGTGAGCTGCAGAGGGAAACG-GCC-3'; reverse 3'-ACACACCTGCGTCTCCCTA-CCTCCACATA-5'
 Tg-2: forward, 5'-AGGGAAACGGCCTTTCTGAA-3'; reverse, 3'-CTTTAGCAGCAGAAGAGGTG-5'
 Tg-3: forward, 5'-GCCTCCATCTGCTGGGTGTC-3'; reverse, 3'-TGGGGTCACAAGACGCCTCCCTC-5'.

Glyceraldehyde 3-phosphate dehydrogenase (*GAPDH*), a ubiquitously expressed control gene, was also analyzed to confirm the success of RNA extraction and the reverse transcription and PCR reactions (4).

This study was approved by the Institutional Review Board.

Venous blood (5–7 mL into an EDTA tube) was collected from 27 healthy individuals (13 males and 14 females), and mononuclear cells were separated by Ficoll-Hypaque gradient. mRNA was extracted with Trizol reagent (Life technologies). One microgram of RNA was reverse-transcribed with the superscript II preamplification system (Invitrogen). PCR was carried out using primers for 30 cycles [94 °C for 1 min (first cycle for 2 min), 62 °C for 1 min, and 72 °C for 1 min (10 min for the last cycle)]. RT-PCR products were resolved by 2% gel electrophoresis and visualized by ethidium bromide staining.

During the initial testing we observed that all four TSHR primer pairs amplified specific signals from the thyroid cancer tissue. However, the three primer pairs targeted to exons 9 and 10 also amplified signals from normal PBMCs (Fig. 1A). In contrast, primer pair TSHR-4 (exons 6–9; product size, 212 bp) failed to amplify any signal in the PBMCs from any healthy individuals tested (Fig. 1A). Similar results were obtained with Tg primer pairs; whereas all Tg primer pairs amplified specific signals from the thyroid tissues, only two of these (Tg-1 and Tg-3) amplified signals from PBMCs of healthy

individuals (data not shown). One primer pair (Tg-2) was specific for thyroid tissue only and showed no reactivity in PBMCs from healthy individuals. On the basis of these findings, the TSHR-4 and Tg-2 primer pairs were selected for further testing in clinical samples and to further refine the sensitivity of these assays.

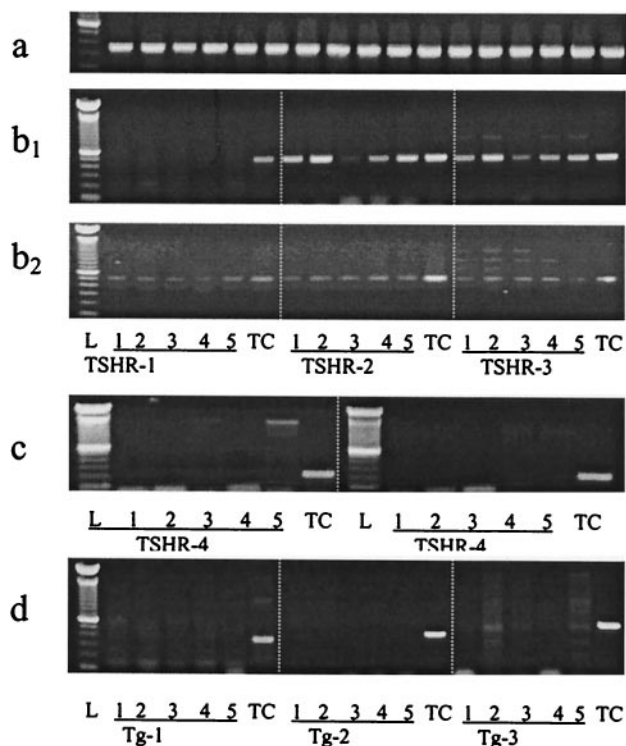
Assay sensitivity was tested by serial dilution of the thyroid cancer tissue RNA with the RNA from normal PBMCs. Assuming 10–20 pg total RNA per thyrocyte, mRNA from ~50–100 cells/mL of blood was detected by ethidium bromide staining. The lower limit of detection was further improved by increasing the template amount from 1 µg to 5 µg and by increasing the number of PCR cycles from 30 to 38. With these modifications, the estimated detection limit was ≤10 cancer cells/mL of blood (Fig. 1). Even with this enhancement in sensitivity, the selected primer pairs for both TSHR-4 and Tg-2 showed no reactivity with PBMCs from healthy individuals when retested.

Clinical validation of these RT-PCR assays was then performed by analyzing blood from 10 healthy euthyroid individuals, 8 patients with benign thyroid diseases, and 27 patients with treated thyroid cancer. All thyroid cancer patients were on thyroid suppressive therapy at the time of testing and had diagnostic WBS within the previous 2 years. Twenty-one of these patients were negative for residual disease, 3 had distant metastases, and 3 showed local recurrences.

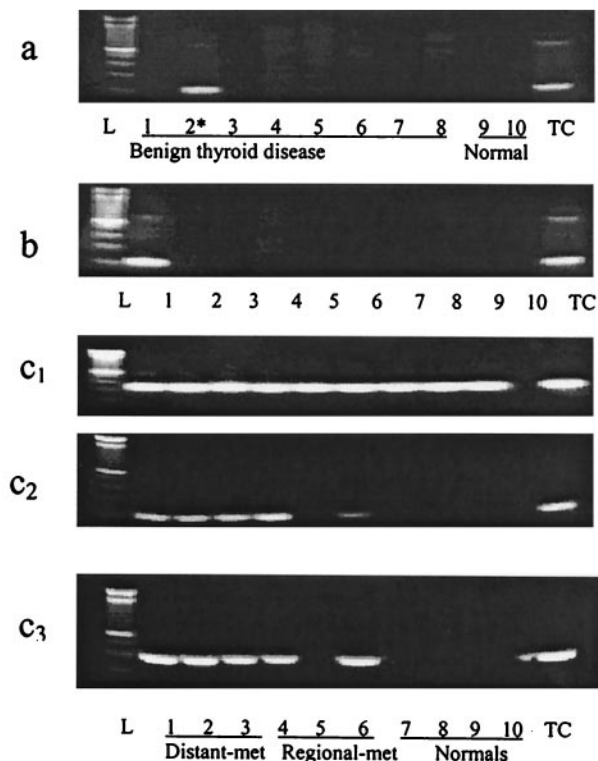
No TSHR or Tg mRNA signals were detected in 10 euthyroid individuals and in 7 of 8 patients with benign thyroid disease (5 with hyperthyroidism and 2 with multinodular goiter). One patient with a large goiter, and tracheal compression was positive for both TSHR and Tg mRNA. TSHR and Tg mRNA were detected in the three patients with distant metastases and in two of the three with thyroid bed/neck uptake [total, five of six (83%)]. Of 21 patients with negative WBS, only one (5%) was positive for both TSHR and Tg mRNA (Fig. 1B and Table 1). Tg mRNA was detected in two more patients with negative WBS whose serum Tg concentrations were undetectable. It remains to be seen whether these three WBS- and serum Tg-negative patients eventually will become positive on follow-up testing, which in turn will confirm the early detection capability of the TSHR and Tg mRNA assay.

Our results suggest that the specificity of RT-PCR depends to a greater extent on the design of the oligonucleotide primers. Like Francis et al. (15), we also detected TSHR transcripts in normal lymphocytes with primers amplifying the exon 10 segment. However, in PBMCs from healthy individuals and patients with benign thyroid diseases, the segment spanning exons 6–9 failed to amplify. Similarly, many investigators have detected Tg mRNA transcripts in blood from healthy euthyroid individuals (7, 8), whereas others failed to detect any signals in blood from healthy individuals (6). Ringel et al. (7) related these differences to the greater sensitivity of their RT-PCR assay. Our results using different primer sets suggest that these differences relate to primer pair selection. Using the same primer pair used by Ringel et al., we

A. TSHR & Tg mRNA in Healthy Controls



B. TSHR & Tg mRNA in Thyroid Diseases



C: Sensitivity of RT-PCR for TSHR and Tg mRNA

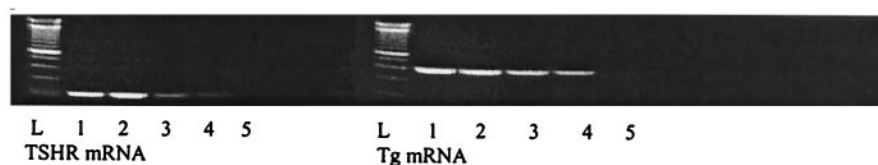


Fig. 1. TSHR mRNA in healthy individuals (A) and patients with thyroid diseases (B).

(A), TSHR mRNA in healthy individuals, detected with different primer pairs. Panel a, GAPDH mRNAs (397 bp). Panels b₁ and b₂, TSHR mRNA from five healthy females (b₁, lanes 1–5) and five healthy males (b₂, lanes 1–5) with use of primer pairs TSHR-1 (498 bp), TSHR-2 (486 bp), and TSHR-3 (503 bp). Panel c, TSHR expression in healthy individuals with use of primer pair TSHR-4 (202 bp). Panel d, Tg mRNA in five healthy individuals with use of three different primer pairs (Tg-1, Tg-2, and Tg-3). (B), TSHR and Tg mRNA in patients with benign thyroid diseases and thyroid cancer. Panel a, patients with benign thyroid diseases (lanes 1–8) and controls (lanes 9 and 10). Panel b, thyroid cancer patients on thyroxine suppression and with negative ¹³¹I scans (n = 21; 10 are shown in lanes 1–10). Panels c₁–c₃ show GAPDH mRNA (c₁), TSHR mRNA (c₂), and Tg mRNA (c₃) in thyroid cancer patients with positive ¹³¹I scans. Shown are patients with distant metastasis (lanes 1–3) or regional metastases (lanes 4–6) and healthy controls (lanes 7–10). (C), sensitivity of RT-PCR for TSHR and Tg. Total RNA from thyroid cancer (lane 1) was diluted with RNA from normal mononuclear cells (1:10, 1:100, 1:1000, 1:10 000; lanes 2–5). L, DNA molecular weight ladder, TC, thyroid cancer tissue RNA; met, metastasis. *, patient with large goiter and tracheal compression.

Table 1. TSHR and Tg mRNA positivity in healthy individuals and patients with benign thyroid disease and thyroid cancer.

	No. tested	No. positive for	
		TSHR (%)	Tg mRNA (%)
Healthy volunteers	10	0 (0)	0 (0)
Benign thyroid disease	8	1 (12)	1 (12)
Thyroid cancer patients			
Negative ¹³¹ I scan	21	1 (5)	3 (14)
Positive ¹³¹ I scan	6	5 (83)	5 (83)

also detected positive signals in some healthy individuals, but failed to do so with another primer pair (even after significant enhancement of sensitivity) that showed specific signals selectively in those thyroid cancer patients with positive scans. As discussed previously by others, the discordance between different primers can be explained by the limitation of PCR-based techniques to detect only the alternatively spliced variants amplified by the selected primers (9, 11).

In summary, our results confirm previous findings that TSHR mRNA is detected by RT-PCR in PBMCs from

healthy individuals. However, we found that this positivity was dependent on the primer pairs used and that, with careful selection of the primer pair, the presence of mRNA was specific for thyroid cancer and corresponded to the presence of extrathyroidal disease and the presence of Tg mRNA transcripts. With further refinement of this assay and with the development of a quantitative real-time PCR procedure, the measurement of TSHR mRNA by RT-PCR may serve as a specific and sensitive tool for monitoring of thyroid cancer.

This study was supported by a grant from The Cleveland Clinic, Research Projects Fund. This work was presented at the 34th Annual Oak Ridge Conference, April 25–26, 2002, La Jolla, CA.

References

- Solomon BL, Wartofsky L, Burman KD. Current trends in the management of well differentiated papillary thyroid carcinoma. *J Clin Endocrinol Metab* 1996;81:333–9.
- Ozata M, Suzuki S, Miyamoto T, Liu RT, Fierro-Renoy F, DeGroot LJ. Serum thyroglobulin in the follow-up of patients with treated differentiated thyroid cancer. *J Clin Endocrinol Metab* 1994;79:98–105.
- Spencer CA, Wang CC. Thyroglobulin reassessment: techniques, clinical benefits, and pitfalls. *Endocrinol Metab Clin North Am* 1995;24:841–63.
- Grasso YZ, Gupta MK, Levin MS, Zippe CD, Klein EA. Combined nested RT-PCR assay for prostate specific antigen and prostate-specific membrane antigen in prostate cancer patients: correlation with pathological stage. *Cancer Res* 1998;58:1456–9.
- Mattano LA, Moss TJ, Emerson SG. Sensitive detection of rare circulating neuroblastoma cells by reverse transcriptase-polymerase chain reaction. *Cancer Res* 1992;52:4701–5.
- Ditkoff BA, Marvin MR, Yemul S, Shi YJ, Chabot J, Feind C, et al. Detection of circulating thyroid cells in peripheral blood. *Surgery* 1996;120:959–65.
- Ringel MD, Ladenson PW, Levine MA. Molecular diagnosis of residual and recurrent thyroid cancer by amplification of thyroglobulin messenger ribonucleic acid in peripheral blood. *J Clin Endocrinol Metab* 1998;83:4435–42.
- Bojunga J, Roddiger S, Stanisch M, Kusterer K, Kurek R, Renneberg H, et al. Molecular detection of thyroglobulin mRNA transcripts in peripheral blood of patients with thyroid disease by RT-PCR. *Br J Cancer* 2000;82:1650–5.
- Wingo ST, Ringel MD, Anderson JS, Patel AD, Lukes YD, Djuh Y, et al. Quantitative reverse transcription-PCR measurement of thyroglobulin mRNA in peripheral blood of healthy subjects. *Clin Chem* 1999;45:785–9.
- Ringel MD, Baldushi-Silano PL, Anderson JS, Spencer CA, Silverman J, Sparling YH, et al. Quantitative reverse transcription polymerase chain reaction of circulating thyroglobulin messenger ribonucleic acid for monitoring patients with thyroid carcinoma. *J Clin Endocrinol Metab* 1999;84:4037–42.
- Savagner F, Rodien P, Reynier P, Rohmer V, Bigorgne JC, Malthiery Y. Analysis of Tg transcripts by real-time RT-PCR in the blood of thyroid cancer patients. *J Clin Endocrinol Metab* 2002;87:635–9.
- Ohta K, Endo T, Onaya T. The mRNA levels of thyrotropin receptor, thyroglobulin, and thyroid peroxidase in neoplastic human thyroid tissues. *Biochem Biophys Res Commun* 1991;165:1250–5.
- Sheils OM, Sweeny EC. TSH receptor status of thyroid neoplasms—TaqMan RT-PCR analysis of archival material. *J Pathol* 1999;188:87–92.
- Arturi F, Russo D, Giuffrida D, Ippolito A, Perrotti N, Vigneri R, et al. Early diagnosis by genetic analysis of differentiated thyroid cancer metastases in small lymph nodes. *J Clin Endocrinol Metab* 1997;82:1638–41.
- Francis T, Burch HB, Cai W, Lukes Y, Peele M, Carr FE, et al. Lymphocytes express thyrotropin receptor-specific mRNA as detected by the PCR technique. *Thyroid* 1991;1:223–8.

Photoaptamer Technology: Development of Multiplexed Microarray Protein Assays, Dom Zichi, Tepper Koga, Chad Greef, Rachel Ostroff, and Helen Petach* (SomaLogic, Inc., 1745 38th St., Boulder, CO 80301; * author for correspondence: fax 303-545-2525, e-mail hpetach@somallogic.com)

To study and identify the complex protein expression patterns associated with a disease, efficient methods are necessary to detect and quantify hundreds of proteins simultaneously, many of which are present in exceedingly low concentrations. Photoaptamers are intriguing capture agents for multiplexed proteomics assays because they demonstrate extraordinary specificity and sensitivity toward protein analytes and can be used in the multiplexed array format. Photoaptamers are single-stranded DNA molecules that have the ability to form covalent bonds with their cognate proteins when they are electronically excited.

Photoaptamers have been discovered for proteins with a wide range of characteristics, including acidic, basic, large, small, glycosylated, chemically modified, and hydrophobic, and these photoaptamers may be used in a wide variety of formats, including most formats available to antibodies (1–5). The photoSELEX process has been successfully automated as a high-throughput process so that a wide range of proteins have yielded active photoaptamers that exhibit nanomolar or better affinities (6–9). The photoaptamers described below were selected for the proteins thrombin and basic fibroblast growth factor (bFGF) (10–13). The sensitivities, specificities, and cross-linking efficiencies of the photoaptamers suggest that they will be suitable capture agents for microarrays. For example, the bFGF photoaptamer has a K_d of ~16 pmol/L, a photo cross-linking yield of 50%, and specific binding to bFGF that is more than three orders of magnitude higher than binding to other heparin-binding proteins, such as vascular endothelial growth factor and platelet-derived growth factor (13). The bFGF photoaptamer characteristics and sequence have been described previously (13).

We identified photoaptamers in vitro by use of the photoSELEX process (12, 14) to select high-affinity sequences from a random pool of oligonucleotides. Photoaptamers were synthesized at SomaLogic, Inc. by use of standard phosphoramidite chemistry (15, 16), with a brominated deoxyuridine substituted for the thymidine (T) usually found in DNA; these photoactive residues participate in covalent bond formation. The photoaptamers were deprotected by use of a mild base to avoid the degradation of the brominated deoxyuridine, a chemically sensitive moiety.

Photoaptamers have previously been shown to cross-link to specific sites on their target proteins, as assessed by Edman and mass spectral sequencing methodologies (17). The array methods described below allowed the parallel assessment of several photoaptamers for both affinity and specificity. They also served as a model for how photoaptamer arrays can be used to measure the concentra-

tions of numerous distinct proteins in a single 100- μ L sample. For the multiplexed assays described below, photoaptamers were synthesized with an amine on the 5' terminus to provide a covalent anchor to an array surface.

Both the thrombin and bFGF photoaptamers were characterized using the same experimental approach as described previously (13). Because photoaptamers are chemically stable and renature readily, harsh conditions, including base, chaotropic agents, and detergents, can be used during immobilization and washing to create high-density aptamer loading with homogeneous orientation and activity.

Amine-substituted photoaptamers were spotted onto Motorola CodeLink activated slide surfaces (25 \times 75 mm) from a phosphate spotting solution at pH 8.5 (containing 150 mmol/L sodium phosphate and 10 μ mol/L oligonucleotide) by use of the Genemachine Accent contact spotter with a Telechem Stealth SMP4B pin. Spots were 100 μ m in diameter and were separated by a spot-to-spot distance of 250 μ m. After 60 min, the slides were finished by soaking in 20 mmol/L NaOH followed by a 0.2 g/L sulfo-NHS-acetate treatment to ensure that residual *N*-hydroxysuccinimide (NHS) and amine reactive groups were capped to prevent further reaction. Microarrays typically contained 200 photoaptamer spots, but could be configured to array from one to hundreds of photoaptamers on a single chip. The microarray was incubated with 100 μ L of the relevant analyte solution (see discussion of multiplexed analytes below), and the analyte solution was flowed across the slide surface in a continuous loop. Photoaptamers have been specifically attached to a variety of surfaces, including multiplexed array surfaces, by incorporating appropriate reactive groups during their synthesis.

After incubation of the binding solution, the microarray was washed in HEPES buffer at pH 7.4 for several minutes to remove nonspecifically bound protein, then the array was irradiated at 308 nm with a XeCl excimer laser to photo cross-link the photoaptamer to its cognate protein. Exposing the protein/aptamer complex to ultraviolet light induces covalent bond formation between the photoaptamer and cognate protein. Harsh denaturing washes were applied to remove any noncovalently bound protein from the array. The microarray was then treated with 6.3 mg/L NHS-Alexa555 for 30 min or other amine-specific reagents coupled to enzymatic or fluorescent probes to label the lysines on the covalently linked proteins.

The processed microarray was read in an Applied Precision ArrayWoRx[®] Biochip Reader to quantify the fluorescence from covalently bound protein on each photoaptamer feature.

Microarrays were incubated with a protein analyte solution containing mixtures of proteins to test the photoaptamers for both specificity and sensitivity. We attempted to ensure that photoaptamers exhibiting nonspecific binding and cross-linking or other interferences were detected and eliminated from the photoaptamer collection by requiring each protein pair to be sampled in two ways:

(*a*) in one solution, one protein was present in excess over the second protein; and (*b*) in the second solution, the second protein was present in excess of the first protein. For eight proteins distributed in eight samples, there are 28 such pairs in each sample (7 comparisons to the photoaptamer with no protein, 6 comparisons for the lowest concentration protein, and so forth). In the current example, each protein pair will differ by at least one log of concentration in at least one solution (on average, two), ensuring that cross-reactivity is detected in the assay.

In this experiment, each cognate protein concentration was varied from 0.01 to 10 nmol/L, whereas seven other proteins were varied over the same concentration range. The total concentration in each microarray experiment was 11.1 nmol/L protein, containing various concentrations of endostatin, bFGF, thrombin, angiogenin, tumor growth factor- β 1, interleukin-4, p-selectin, and serum amyloid p component.

To assess the quality of photoaptamers for binding to a specific protein target, the experiments must include two key qualities that are required for use on a proteomics chip: the dynamic range of the linear response and assessment of specificity. A multiplex assay for such an evaluation would allow for greater efficiency than testing photoaptamers in individual experiments.

To assess surface activity of the photoaptamers, eight-point binding curves for each photoaptamer were generated. The multiplexed analyte solutions were used to simultaneously evaluate dose-response curves for photoaptamers to eight protein targets using eight complex solutions. Specific binding curves are shown for both the thrombin photoaptamer and bFGF photoaptamer. The images of the microarray (Fig. 1A) illustrate the increasing signals on photoaptamer features in response to increasing cognate protein concentrations. The quantification of the microarray images yielded the protein binding curves below (Fig. 1B). The presence of multiple analytes during binding incubation on the array does not alter the specific binding curve for the cognate photoaptamer. The thrombin binding curve to its cognate aptamer demonstrates a limit of detection of 100 pmol/L; this limit was determined by slide background (noise), not the capabilities of the photoaptamers as capture agents.

Because each of the analyte solutions contained a different high-concentration protein, the binding curves demonstrate specificity of the photoaptamer reaction to its cognate protein. Nonspecific binding would be evident if some points along the binding curve were dramatically displaced, indicating that a noncognate protein interacted with the photoaptamer. The binding curves in this experiment (Fig. 1B) demonstrate specific binding between photoaptamer and cognate protein.

Because many photoaptamers to the same cognate protein can be arrayed together, the performance of those individual photoaptamers can be compared directly for selection of the most sensitive and specific photoaptamer to a protein target. Specificity can be determined over a wide range of concentrations of noncognate proteins without evidence of interference.

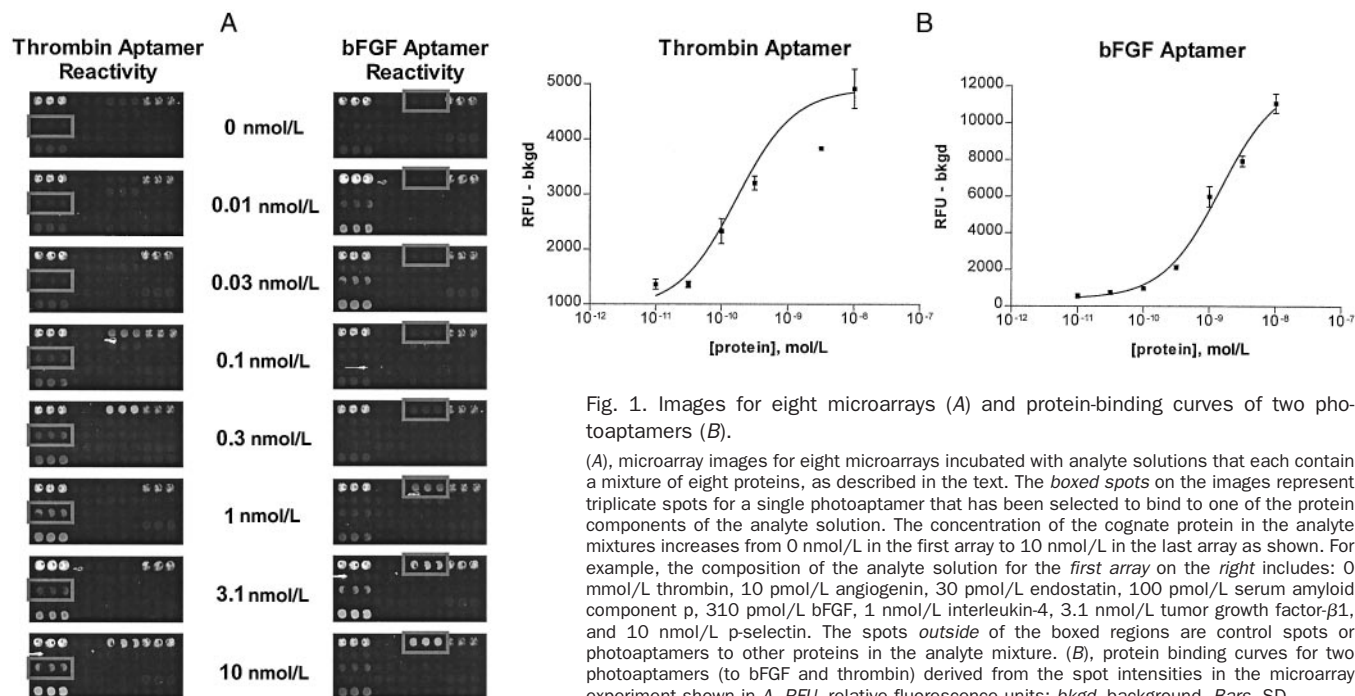


Fig. 1. Images for eight microarrays (A) and protein-binding curves of two photoaptamers (B).

(A), microarray images for eight microarrays incubated with analyte solutions that each contain a mixture of eight proteins, as described in the text. The boxed spots on the images represent triplicate spots for a single photoaptamer that has been selected to bind to one of the protein components of the analyte solution. The concentration of the cognate protein in the analyte mixtures increases from 0 nmol/L in the first array to 10 nmol/L in the last array as shown. For example, the composition of the analyte solution for the first array on the right includes: 0 mmol/L thrombin, 10 pmol/L angiogenin, 30 pmol/L endostatin, 100 pmol/L serum amyloid component p, 310 pmol/L bFGF, 1 nmol/L interleukin-4, 3.1 nmol/L tumor growth factor- β 1, and 10 nmol/L p-selectin. The spots outside of the boxed regions are control spots or photoaptamers to other proteins in the analyte mixture. (B), protein binding curves for two photoaptamers (to bFGF and thrombin) derived from the spot intensities in the microarray experiment shown in A. RFU, relative fluorescence units; bkgd, background. Bars, SD.

The alluring feature of microarrays is the multiplexing capacity, which yields massively parallel analysis of complex mixtures of proteins from serum, plasma, cell lysates, and even tissue extracts separated by laser capture dissection (18). The advantages of using photoaptamers in microarrays instead of multiplexed antibodies are many, most notably their ease of manipulation and the elimination of cross-reactivity associated with the second dimension of an ELISA.

High specificity in a photoaptamer array is achieved by combining the intrinsic affinity of a photoaptamer for its target protein with the demand for photoactivated cross-linking between the brominated deoxyuridine in the photoaptamer and a specific amino acid residue of the target protein. The additional specificity of the second dimension (photo cross-linking) derives from the requirement that the target amino acid must be positioned appropriately both in distance and orientation to yield the covalent bond (13,19). In this sense, the photo cross-linking event provides a second level of specificity analogous to the secondary antibody of an ELISA.

In addition to adding specificity to protein/aptamer pairs, the photoactivated covalent cross-linking effectively attaches each analyte molecule to its appropriate address on a microarray surface. The cross-link is stable to stringent wash conditions, allowing the removal of non-specifically bound proteins before labeling and detection. The result should improve limits of detection and quantification, which will make protein microarrays truly useful tools by enabling the parallel measurement of even low-abundance proteins. Experiments are underway to test these arrays in complex biological solutions, but those data are not presented here.

Because photoaptamers are nucleic acids, a simple

universal protein stain can be used to generate signal. A universal protein stain will chemically couple to protein moieties, e.g., lysine residues, with virtually no reactivity to photoaptamer features. This unique approach allows a single binding event, rather than a "sandwich" to generate sensitive, specific results in a multiplex array format. In the absence of the photo cross-linking event, we expect the background of the assay to be increased and adversely affect the lower limit of detection.

Arrays containing from one to hundreds of photoaptamers can be readily created for a wide variety of protein targets by use of the PhotoSELEX process for photoaptamer selection and the array protocols developed for those photoaptamers. These arrays should scale to any feature density without complications caused by secondary antibodies.

We thank the following individuals for their contributions to the assay experimental work: Steve Buhl, Steve Tyrrell, Jim Heil, Greg Husar, Drew Smith, and Glenn Foulds.

References

1. Davis KA, Abrams B, Lin Y, Jayasena SD. Use of a high affinity DNA ligand in flow cytometry. *Nucleic Acids Res* 1996;24:702-6.
2. Drolet DW, Moon-McDermott L, Romig TS. An enzyme-linked oligonucleotide assay [see comments]. *Nat Biotechnol* 1996;14:1021-5.
3. Morris KN, Jensen KB, Julin CM, Weil M, Gold L. High affinity ligands from in vitro selection: complex targets. *Proc Natl Acad Sci U S A* 1998;95:2902-7.
4. Ringquist S, Parma D. Anti-L-selectin oligonucleotide ligands recognize CD62L-positive leukocytes: binding affinity and specificity of univalent and bivalent ligands. *Cytometry* 1998;33:394-405.
5. Romig TS, Bell C, Drolet DW. Aptamer affinity chromatography: combinatorial chemistry applied to protein purification. *J Chromatogr B Biomed Sci Appl* 1999;731:275-84.
6. Lee M, Walt DR. A fiber-optic microarray biosensor using aptamers as receptors. *Anal Biochem* 2000;282:142-6.
7. Brody EN, Willis MC, Smith JD, Jayasena S, Zichi D, Gold L. The use of

- aptamers in large arrays for molecular diagnostics. *Mol Diagn* 1999;4:381–8.
8. Brody E, Gold L. Aptamers as therapeutic and diagnostic agents. *Rev Mol Technol* 2000;74:5–13.
 9. Jayasena S. Aptamers: an emerging class of molecules that rival antibodies in diagnostics. *Clin Chem* 1999;45:1628–50.
 10. Jensen KB, Atkinson BL, Willis MC, Koch TH, Gold L. Using in vitro selection to direct the covalent attachment of human immunodeficiency virus type 1 Rev protein to high-affinity RNA ligands. *Proc Natl Acad Sci U S A* 1995;122:20–4.
 11. Drolet DW, Jenison RD, Smith DE, Pratt D, Hicke BJ. A high throughput platform for systematic evolution of ligands by exponential enrichment (SELEX). *Comb Chem High Throughput Screen* 1999;2:271–8.
 12. Mullah B, Livak K, Andrus A, Kenney P. Efficient synthesis of double dye-labeled oligodeoxyribonucleotide probes and their application in a real time PCR assay. *Nucleic Acids Res* 1998;26:1026–31.
 13. Cobb CJ, Scott G, Swingler RJ, Wilson S, Ellis J, MacEwen CJ, et al. Rapid mutation detection by the transgenomic wave analyser DHPLC identifies MYOC mutations in patients with ocular hypertension and/or open angle glaucoma. *Br J Ophthalmol* 2002;86:191–5.
 14. Golden MC, Resing RA, Collins BC, Willis MC, Koch TH. Mass spectral characterization of a protein-nucleic acid photocrosslink. *Protein Sci* 1999;8:2806–12.
 15. Jones MB, Krutzsch H, Shu H, Zhao Y, Liotta LA, Kohn EC, et al. Proteomic analysis and identification of new biomarkers and therapeutic targets for invasive ovarian cancer. *Proteomics* 2002;2:76–84.
 16. Golden MC, Collins BD, Willis MC, Koch TH. Diagnostic potential of PhotoSELEX-evolved ssDNA aptamers. *J Biotechnol* 2000;81:167–78.
 17. Meisenheimer KM, Meisenheimer PL, Koch TA. Nucleoprotein photocrosslinking using halopyrimidine-substituted RNAs. *Methods Enzymol* 2000;318:88–104.
 18. Hesselberth J, Robertson MP, Jhaveri S, Ellington AD. In vitro selection of nucleic acids for diagnostic applications. *J Biotechnol* 2000;74:15–25.
 19. Zhai G, Iskandar M, Barilla K, Romaniuk PJ. Characterization of RNA aptamer binding by the Wilms' tumor suppressor protein WT1. *Biochemistry* 2001;40:2032–40.